Thermally and mechanically robust self-healing supramolecular polyurethanes featuring aliphatic amide end caps

Tareq, A. Z., Hyder, M., Hermida Merino, D., Chippindale, A. M. ORCID: https://orcid.org/0000-0002-5918-8701, Kaur, A., Cooper, J. A. ORCID: https://orcid.org/0000-0002-3981-9246 and Hayes, W. ORCID: https://orcid.org/0000-0003-0047-2991
(2024) Thermally and mechanically robust self-healing supramolecular polyurethanes featuring aliphatic amide end caps. Polymer, 302. 127052. ISSN 1873-2291 doi: 10.1016/j.polymer.2024.127052 Available at https://centaur.reading.ac.uk/116032/

Polymer 302 (2024) 127052

Contents lists available at ScienceDirect

Polymer

journal homepage: www.elsevier.com/locate/polymer

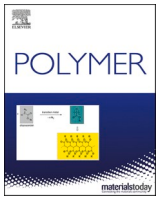

Thermally and mechanically robust self-healing supramolecular polyurethanes featuring aliphatic amide end caps

Alarqam Z. Tareq [a], Matthew Hyder [a], Daniel Hermida Merino [b], Ann M. Chippindale [a], Amanpreet Kaur [c], James A. Cooper [a], Wayne Hayes [a,*]

[a] Department of Chemistry, University of Reading, Whiteknights, Reading, RG6 6DX, UK
[b] DUBBLE CRG, BM26, ESRF-The European Synchrotron, Netherlands Organization for Scientific Research, 6 Rue Jules Horowitz, 38043, Grenoble, France
[c] Centre for Advanced Microscopy, Chemical Analysis Facility, University of Reading, Whiteknights, Reading, RG6 6ED, UK

ARTICLE INFO

Keywords:
Supramolecular polymer
Hydrogen bonding
Thermal and mechanical reinforcement
Self-healing
Amide functionality

ABSTRACT

A series of supramolecular polyurethanes (SPUs) were designed and synthesised with synergetic multifunctional hydrogen bonding aliphatic amide end-caps. Hydrogen bonding between the urethane, urea, and amide motifs in the polymers afford strong dynamic association between polymer chains in the solid state. Phase separation of the apolar and polar components of the polyurethanes also serves to reinforce their thermal and mechanical properties. The supramolecular polyurethane with bisamide-morpholine end caps associates via multiple hydrogen bonds and exhibits enhanced tensile and thermal properties when compared to the other materials. Variable-temperature infrared spectroscopy (VT-IR) and atomic force microscopy (AFM), were carried out to study the phase morphology of the polymers and revealed a correlation between increased phase separation and the introduction of amide motifs in the end-caps. These SPUs also exhibit excellent healing abilities, requiring temperatures >200 °C to recover their physical properties.

1. Introduction

Supramolecular chemistry has provided an effective and powerful approach for the creation of stimuli-responsive materials by employing highly directional and reversible non-covalent interactions, such as hydrogen bonding [1–3], donor–acceptor interactions (e.g. π− π stacking) [4–6], host–guest interactions [7,8], metal–ligand interactions [9,10] and van der Waals' forces of attraction [11,12] between the monomeric subunits. The dynamic dissociation/re-association of such non-covalent bonds has led to supramolecular materials capable of self-healing [13] and shape recovery [14]. Responsive behaviour and attenuation of the physical properties of these self-assembled materials can be induced upon exposure to external stimuli, such as light [15], heat [16–18], magnetic fields [19], oxidation–reduction processes [20] and changes in pH [21,22]. For example, Lee and co-workers reported the generation of healable iontronic supramolecular adhesives which are constructed from gel-elastomer crosslinked systems via adhesive electrodes (ionic organohydrogel) with a polyurethane as a dielectric layer [23]. Cooper et al. have synthesised a tough and stretchable polymer via one-pot synthesis — this material had shape-memory properties based on the formation of a strain-induced supramolecular nanostructure that enhanced the high energy density of the polymer [24].

Supramolecular polymers have been realised by the introduction of the non-covalent interactions mentioned above into polymer networks through functionalised end-caps [25], pendant groups [26], or linkers [27] to provide these materials with unique tailorable properties. These dynamic properties have led to the application of these supramolecular polymer systems in numerous fields, such as biomedicine [28,29], 3D printing [30,31], controlled drug delivery systems [32–34], coatings [35,36] and adhesives [37,38]. Notably, Meijer and co-workers designed and generated a high-molecular-weight supramolecular polymer in dilute solution by the self-assembly of bifunctional end-capped oligomers bearing ureidopyrimidone (UPy) units that associated via complementary quadruple hydrogen bonds [39,40]. Zhu et al. prepared a self-healing polyurethane with self-complementary quadruple

* Corresponding author.
E-mail addresses: a.z.tareq@pgr.reading.ac.uk (A.Z. Tareq), m.hyder@pgr.reading.ac.uk (M. Hyder), daniel.hermida_merino@esrf.fr (D.H. Merino), a.m.chippindale@reading.ac.uk (A.M. Chippindale), amanpreet.kaur@reading.ac.uk (A. Kaur), james.cooper@reading.ac.uk (J.A. Cooper), w.c.hayes@reading.ac.uk (W. Hayes).

https://doi.org/10.1016/j.polymer.2024.127052
Received 18 December 2023; Received in revised form 14 March 2024; Accepted 11 April 2024
Available online 14 April 2024

hydrogen bonding units that enhanced the self-healing and shape recovery properties via hydrogen bonding [41].

There are several important factors which are essential for the commercialization of such materials. For example, the availability and simplicity of synthesis are two major considerations [42,43]. Polyurethanes (PU) are generally considered to be commercially viable materials as a result of their tailorable properties, scalability and the simplicity of their synthesis [44]. PUs are comprised of specific stoichiometric ratios of hard domains (typically derived from diisocyanates), which have a significant influence on the physical characteristics, such as ultimate tensile strength and mechanical performance of the final products [45] and soft domains (arising from the polyol feed), which can provide desirable elastic characteristics [46,47].

We have previously reported several supramolecular polyurethane (SPU) systems that self-assemble efficiently via hydrogen bonding in combination with phase-separation phenomena which are capable of healing [16,48,49]. In one example, the recovery of the mechanical properties post damage was observed within 60 min after the film was exposed to a temperature of only 37 °C (human body temperature) [37]. This polyurethane was designed to combine hydrogen bonding and aromatic π− π stacking forces which resulted in phase separation in the bulk to facilitate network assembly. Merino et al. have reported bisurethane and bisurea functionalised polymers, which associate via hydrogen-bonding networks and self-assemble into thermally responsive elastomeric materials [50].

Herein we report a series of novel SPUs which are designed to utilize a combination of non-covalent interactions and phase separation to afford dynamic supramolecular materials for use as healable coatings. Hydrogen-bonding motifs have been introduced in the form of urea and amide functionalised end-caps, in conjunction with π− π interactions between the aryl units within 4,4′-methylene bis phenyl isocyanate (4,4′-MDI), to develop thermal stable polymers with self-healing properties. In addition, this study aimed to explore how the amides can play a key role in reinforcing the rheological, thermal, and mechanical properties of supramolecular polyurethanes.

2. Experimental

2.1. Materials

Krasol™ HLBH-P 2000 (molecular weight as supplied = 2100 g mol^{-1}) was kindly provided by Total Cray Valley, all other reagents used were purchased from Sigma Aldrich, TCI, Acros Organics, Fisher Chemical and Fluorochem. The solvents THF and $CHCl_3$ were dried by using an MBRAUN SP7 system fitted with activated alumina columns.

2.2. Characterisation

^{1}H NMR and ^{13}C NMR spectra were measured using either a Bruker Nanobay 400 or a Bruker DPX 400 spectrometer operating for ^{1}H NMR (400 MHz) or ^{13}C NMR (100 MHz) spectroscopic analysis. Chemical shifts (δ) are reported in ppm relative to $CDCl_3$ (δ 7.26 ppm) and the residual solvent resonance (δ 2.50 ppm) for DMSO-d_6, (δ 1.94) CD_3CN, and (δ 1.73 ppm) THF-d_8 in ^{1}H NMR spectra. Fourier-Transform Infrared (FT-IR) spectroscopic analysis was carried out at room temperature using a PerkinElmer 100 FT-IR instrument equipped with a diamond-ATR sampling accessory. Variable-temperature IR (VT-IR) spectroscopic analysis was carried out over the temperature range 20–200 °C using a PerkinElmer 100 FT-IR spectrometer with a Specac variable-temperature cell holder and Temperature Controller. Each sample was analysed as a potassium-bromide disc with a material loading of 1 % wt. The temperature was measured locally with a thermocouple embedded inside the solid-cell frame. The resulting spectra were analysed using the PerkinElmer spectrum IR software (version 10.6.2). Mass spectrometry (MS) was conducted using a Thermo Fisher Scientific Orbitrap XL LCMS. The sample was introduced by liquid chromatography (LC) and sample ionization achieved by electrospray ionization (ESI). The average molecular weights of the polymers generated were determined via Gel Permeation Chromatography (GPC) using the Agilent Technologies 1260 Infinity I system in HPLC-grade THF at a flow rate of 1.0 mL min^{-1}. Calibration was achieved using a series of near monodisperse polystyrene standards and samples were prepared at a concentration of 1.0 mg mL^{-1}. Differential calorimetry (DSC) measurements were performed on a TA Instruments DSC Q2000 adapted with a TA Refrigerated Cooling System (RCS90), using aluminium TA Tzero pans and lids, measuring from −80 °C to 250 °C with heating and cooling rates of 5 °C min^{-1} under nitrogen gas with a flow rate of 50 mL min^{-1}. Thermogravimetric analysis (TGA) was carried out on TA Instruments TGA Q50 instrument with aluminium Tzero pans. The sample was heated from 20 °C to 550 °C at 10 °C min^{-1} under nitrogen gas with a flow rate of 60 mL min^{-1}. Thermal characterisation of samples was investigated using the TA Instruments Universal Analysis 2000 software (version 4.5A). Rheological measurements were performed on a Malvern Panalytical Kinexus Lab + instrument fitted with a Peltier plate cartridge and 8 mm parallel plate geometry and analysed using rSpace Kinexus v1.76.2398 software. Tensile tests were carried out using a Thümler Z3-X1200 tensometer at a rate of 10 mm min^{-1} with a 1 kN load cell and analysed using THSSD-2019 software. Optical microscopy images and video were captured using a Leica DM1000 microscope equipped with a Mettler Toledo FP82 hot stage. The sample was placed onto a glass slide and then placed into the hot stage chamber, the temperature of which is controlled by an FP90 Central Processor (heating rate 10 °C min^{-1}). All videos and images were recorded using Studio86Designs software.

Crystals of **4a-4f** were mounted under Paratone-N oil and flash cooled to 100 K under nitrogen in an Oxford Cryosystems Cryostream. Single-crystal X-ray intensity data were collected using a Rigaku XtaLAB Synergy diffractometer (Cu K_α radiation ($\lambda = 1.54184$ Å)). The data were reduced within the CrysAlisPro software [51]. The structures were solved using the program Superflip [52], and all non-hydrogen atoms were located. Least-squares refinement against F was carried out using the CRYSTALS suite of programs [53]. The non-hydrogen atoms were refined anisotropically. All the hydrogen atoms were located in difference Fourier maps. The positions of the hydrogen atoms attached to nitrogen were refined with a U_{iso} of ~1.2–1.5 times the value of U_{eq} of the parent N atom. The hydrogen atoms attached to carbon were placed geometrically with a C–H distance of 0.95 Å and a U_{iso} of ~1.2–1.5 times the value of U_{eq} of the parent C atom, and the positions refined with riding constraints. Small-angle X-ray scattering (SAXS) and Wide-angle X-ray scattering (WAXS) experiments were performed on a Bruker Nanostar instrument. Samples were mounted in modified DSC pans equipped with Kapton™ windows and mounted in an MRI electrical heating unit for temperature control. The atomic force microscopy (AFM) was conducted in the Centre for Advance Microscopy (CfAM) at the University of Reading using the Cypher S AFM (Oxford Instruments-Asylum Research, Santa Barbara, USA). The AFM stage movement within the x, y and z directions were controlled using piezoelectric stacks. The scans were recorded through the user interface, Igor Pro (Version 16.33.234), using the standard Alternating Contact (AC) Topography mode (tapping mode) operating in air using a silicon tip with a resonant frequency set at approximately 70 kHz and a spring constant of approximately 2.0 Nm^{-1} (AC240TS-R3, Oxford Instruments). Each sample was dropped cast onto a 10 mm diameter AFM mica disc, first cleaved with Sellotape. Each disc was mounted onto 15 mm diameter magnetic stainless steel AFM specimen discs using 9 mm diameter carbon adhesive tabs and secured onto the microscope scanner stage magnetically. Then, through the user interface, the objective focus was adjusted and set to focus on the tip and on each sample in turn. The cantilever was autotuned at its resonance which automatically determined the drive amplitude and drive frequency. The resolution, scan rate, integral gain and scan size (either 2 μm × 2 μm or 10 μm × 10 μm) was entered into the user interface before starting the scan. The software Gwyddion (version 2.63) was used for data analysis and editing. The

synthesis and characterisation data of the compounds and polymers described in this paper are reported in the Supporting Information (SI) file.

3. Results and discussion

3.1. End-cap design

In order to assess the effect of the aliphatic amide end-caps on the mechanical, rheological and thermal properties of the supramolecular polyurethanes together with their self-healing behaviour, novel amino aliphatic end-caps with amide functionalities were designed and synthesised (see Scheme 1). These end-caps have two different end groups; namely, ethyl-morpholine and alkyl units. γ-Aminobutyric acid (GABA) was first protected via a solvent-free condensation with phthalic anhydride to afford the corresponding phthalimide, **1**, 4-(1,3-dioxoisoindolin-2-yl) butanoic acid [54,55]. The formation of the desired amide groups in **2a-2d** was achieved through coupling of the phthalimide **1** and the corresponding amine using *N*-ethyl-*N*′-(3-dimethylaminopropyl) carbodiimide hydrochloride (EDC·HCl) and 4-(dimethylamino)pyridine (DMAP). Subsequent deprotection of the phthalimide protected amine using hydrazine monohydrate afforded the desired amines **3a-3d**. The synthetic protocols used to afford novel end-caps **3a-3d** and their precursors, **1** and **2a-2d**, together with the associated characterisation data, are provided in the SI (see Figs. S1–S18).

3.2. Solid-state structures of end-caps

To gain an insight into the association and assembly of end-caps **3a-3d**, together with the 4-(2-aminoethyl) morpholine and *n*-butylamine, small molecule analogues were synthesised to mimic the polymer end-caps. The amine functionalised end-caps were reacted with 1 equivalent of phenyl isocyanate to form the corresponding ureas, **4a-4f**, as shown in Fig. 1 and Figs. S19–S30. The reactions were monitored by FTIR spectroscopy to observe the consumption of the isocyanate and the formation of the corresponding urea bands. Crystals of the model ureas **4a-4f** were grown via vapour diffusion or slow evaporation and were studied by single crystal X-ray crystallographic analysis (see the SI file for the solid-state structures, hydrogen bonding interactions, and the associated crystallographic data, Figs. S49–S64 and Tables S1–S17). The solid-state structures of the end-caps **4c**, **4e** and **4f** reveal hydrogen bonds between amide–urea and amide–amide groups in head-to-tail type arrangements of the individual molecules. If these interactions and the orientation of the end groups are translated to the assembly of the supramolecular polymers, then the phase separation and association between the polymer chains could be enhanced and lead to reinforcement of the mechanical and rheological properties.

3.3. Synthesis of supramolecular polyurethanes

Five new supramolecular polyurethanes were designed and successfully fabricated using the one-pot, two-step protocol [3,38,45,56] shown in Scheme 2. The synthesis of **SPU1,** has been reported previously [37]. Hydrogenated poly(butadiene) (Krasol HLBH-P 2000) (1.00 equiv.) was reacted with 4,4′-methylenediphenyl diisocyanate (4, 4′-MDI) (2.05 equiv.) for 3 h at 80 °C in the bulk to generate the isocyanate terminated polyurethane pre-polymer (NCO:OH ratio of 2.05:1). The isocyanate-terminated pre-polymer was then solvated in THF or $CHCl_3$ before being reacted with the amine-functionalised end groups (2.05 eq.) for 18 h at 60 °C to afford the resulting SPUs (**SPU1**-**SPU6**) in good yield, as shown in Scheme 2 and Table 1. FTIR spectroscopy was used to monitor each reaction, and when the isocyanate band at 2273-2250 cm^{-1} disappeared, the reaction was considered complete. The SPUs were then isolated after precipitating into ice-cold methanol.

A combination of FTIR, ^{1}H NMR, and ^{13}C NMR spectroscopic analysis was used to confirm the incorporation of the end-caps into **SPU1**-**SPU6**. The ^{1}H NMR spectra of the SPUs reveals four resonances at *ca.* 8.50 ppm, *ca.* 7.80/5.60 ppm, and *ca.* 7.10 ppm, which correspond to the protons in the urethane of the pre-polymer, in the urea and in the amide units of the multifunctional end-cap derivatives, respectively. ^{13}C NMR spectroscopy of the SPUs corroborated the formation of the urethane, urea and amide linkages in the SPUs with resonances observed at *ca.* 154.5, 156.5 and 173.0 ppm, respectively. In addition, new absorbance bands were observed at 1636–1641, 1667 and 1704-1708 cm^{-1} in the FTIR spectra attributed to the carbonyl stretches of the amide, urea and urethane groups, respectively. GPC analysis of the SPUs was used to establish the low degree of chain-extension and confirmed that all of the SPUs have an average of 2–4 hydrogenated poly(butadiene) residues per supramolecular polymer (see Table 1 and Figs. S31–S48), consistent with the analyse of the integral ^{1}H NMR spectra and previous reports [57–59]. The appearance of the casted SPUs films was various as a result to increase the phase separation via hydrogen bonding, see Fig. S93. **SPU2**, **SPU3**, **SPU5**, and **SPU6** possess high M_w and high Đ values — this data can be attributed to the aggregation of the polymer chains as a result of strong intermolecular associations in viscous solution, see Figs. S65–S70.

The thermal properties of the SPUs were studied using TGA and DSC, as shown in Table 1 and Figs. S71–S82. TGA analysis was used to determine the maximum processing temperature by heating the samples

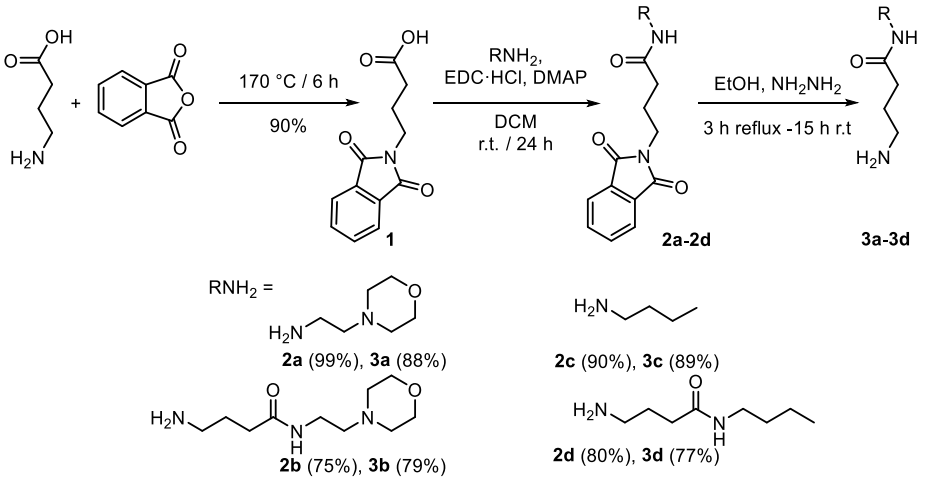

Scheme 1. Synthesis of the novel end-caps **3a-3d**.

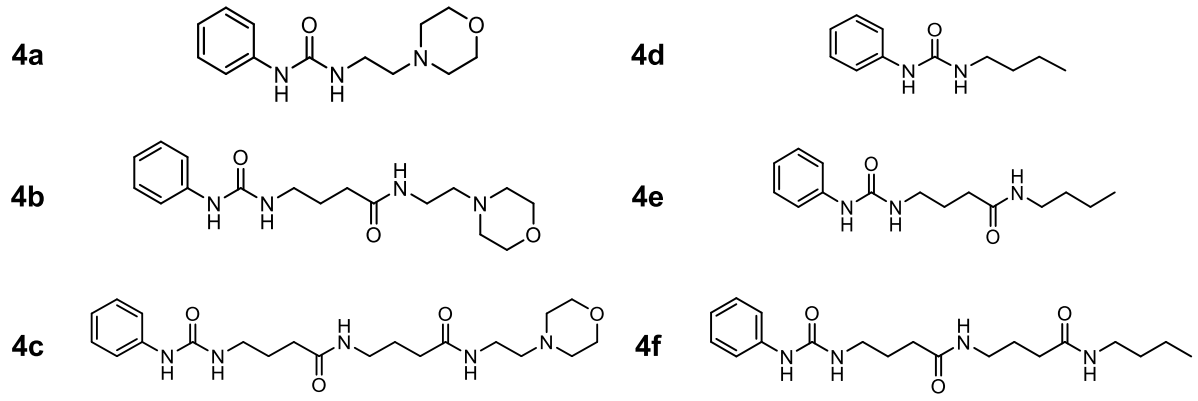

Fig. 1. The structures of the end-cap mimics.

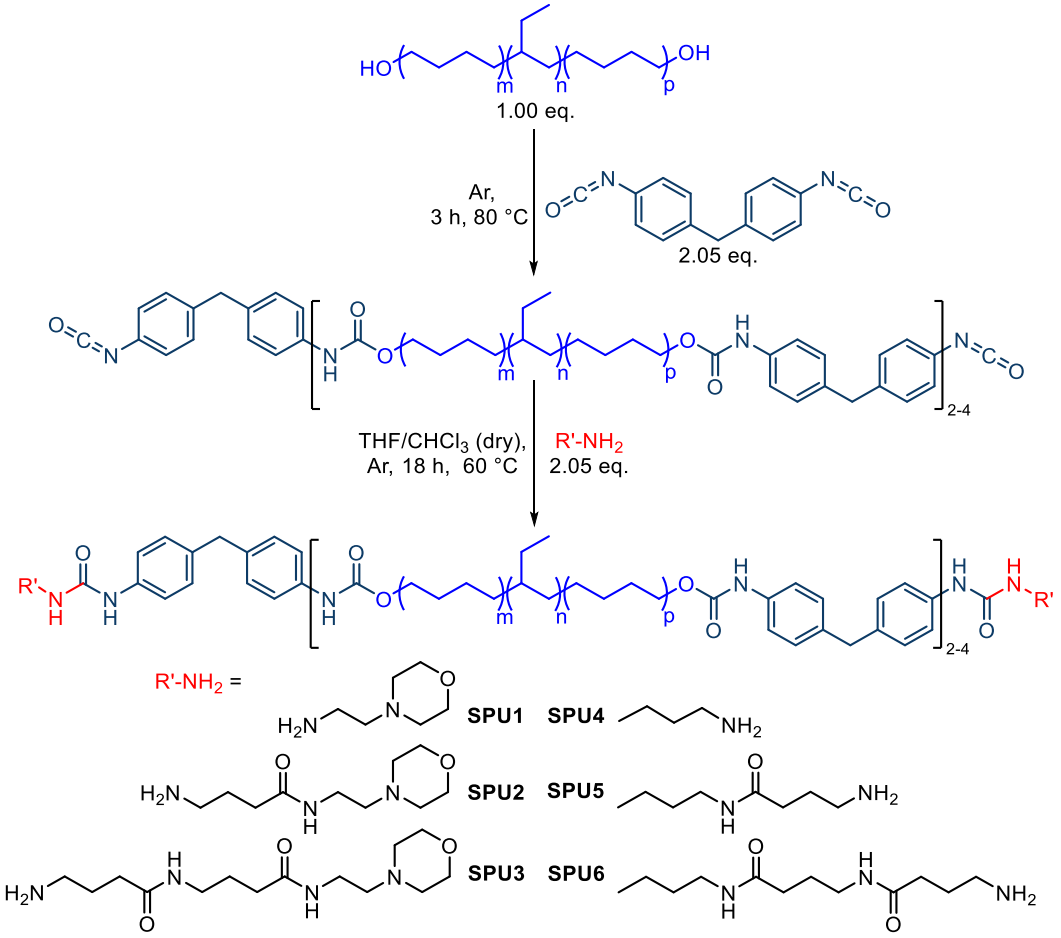

Scheme 2. The synthetic route used to generate the supramolecular polyurethanes **SPU1-SPU6**.

from 20 °C to 550 °C at a rate of 10 °C min^{-1} under a nitrogen atmosphere. All the SPUs exhibited excellent thermal stability under this testing regime and the temperature corresponding to 5 wt% loss was shown in Table 1. Significant degradation did not occur until *ca.* 200 °C and they had degraded fully by 475 °C. Fig. 2 shows the DSC thermogram for each SPU during the first heating cycle. All of the SPUs revealed a glass transition temperature (T_g) at *ca.* −46.5 °C, which is characteristic of the amorphous hydrogenated poly(butadiene) soft segment in the SPU backbone [3,38]. **SPU1** did not show a melt transition within the temperature regime tested [37]. **SPU2** noticed a strong melt transition (T_m) at 195.9 °C attributed to the melting of the hard regions of the polymer chains, and change the state of polymer from viscoelastic solid to viscoelastic liquid. However, with two amide groups present in the end-cap of **SPU3,** this melt transition (T_m) shifted to 235.9 °C as a result of strong hydrogen bonds between urethane, urea, and amide functionalities in adjacent polymer chains. In addition, a broad melt transition was observed at *ca.* 160.3 °C owing to the melting of the hard domains. **SPU5** exhibited two weak and one strong endothermic transitions, the first at 87.5 °C and the second at 104.9 °C, which could correspond to the relaxation of the highly ordered soft segments of the

Table 1
Molecular weight and thermal properties of the supramolecular polymers **SPU1**-**SPU6**.

SPU (% yield	M_n (g mol^{-1})	M_w (g mol^{-1})	Đ	T_d 5 % (°C)	T_g (°C)[b]	T_m (°C)[a]	T_m (°C)[b]
SPU1 (83 %)	7700	15000	1.97	262.6	−46.4	–	–
SPU2 (84 %)	9300	24000	2.56	288.6	−46.2	195.9	–
SPU3 (76 %)	10400	79000	7.60	275.1	−46.2	160.3 235.9	–
SPU4 (78 %)	8152	12280	1.50	307.2	−46.1	56.9 214.9	–
SPU5 (79 %)	11686	24097	2.06	288.6	−46.6	87.5 104.9 235.5	159.4
SPU6 (85 %)	9311	26572	2.85	269.9	−46.1	113.7 191.1 237.8	–

[a] First heating run 5 °C min^{-1}.
[b] Second heating run 5 °C min^{-1}.

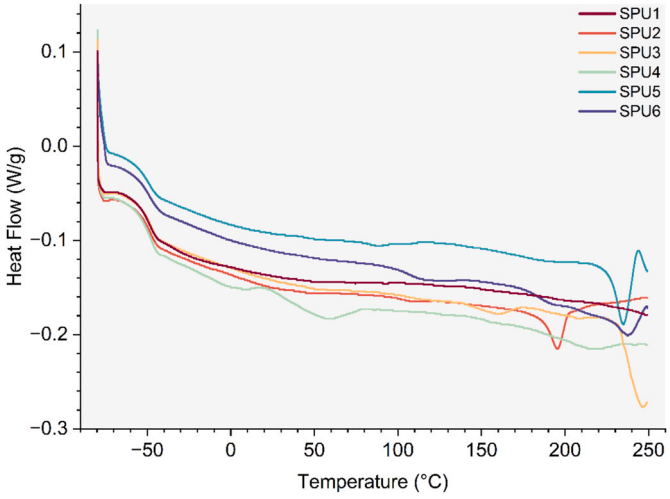

Fig. 2. DSC thermograms of the first heating cycle of **SPU1**-**SPU6** from −80 °C - 250 °C at a heating rate of 5 °C min^{-1}.

hydrogenated poly(butadiene) backbone and disruption of the hard segments formed from the hydrogen-bonded assemblies of the urethane and urea–amide end groups, respectively [3]. The strong melt transition at 235.5 °C revealed to change the physical state of polymer to viscoelastic liquid. Two broad melt transitions at 113.7 °C and 191.1 °C was observed for **SPU6** that was attributed to the melt of the hard regions which were formed via hydrogen bonds between the carbonyl moieties and the N–H units in the amide–urea and amide–amide associations. In addition, a strong melt transition was noticed at 237.8 °C corresponding to the change of the polymer state to viscoelastic liquid. **SPU4** presented two melt transitions, the first one was broad at *ca*. 56.9 °C which can be attributed to dissociation/re-association thermo-reversible crosslinking between the chains in the polymer [60]. The second transition was strong and attributed to change the state of polymer to viscoelastic liquid. All the melt transitions of **SPU1**-**SPU6** that observed in DSC thermograms were agreed well with the HSM results.

In order to study the effect of the end-cap functionality on the microphase separation, thermal, and mechanical properties of the SPUs, rheological analysis and tensile tests were undertaken. In all the cases, rheological measurements were tested in the range from 0 °C up to a maximum temperature of 200 °C, see Figs. S83–S88. Fig. 3 shows the storage modulus (G′) (Fig. 3A) and tan delta (δ) (Fig. 3B) plotted against temperature.

In the temperature regime from 0 °C to 90 °C, **SPU2**, **SPU3**, **SPU5**, and **SPU6** exhibit elastic rubbery properties: the storage modulus stayed constant at the plateau between 10^6-10^7 Pa and then decreased gradually with increasing temperature. This trend indicates the strong association between polymer chains because of the abundance of hydrogen-bonding interactions formed via the urea, amide, and urethane groups, together with the π–π stacking interactions from the MDI units. A similar observation was made by Hyder et al. for a polymer comprised of the same pre-polymer, but with 2-methyl-3-nitroaniline as the end group, which exhibited similar rheological characteristics [38]. **SPU1** shows a simple relaxation with an onset at 37 °C in the G′ as a result of the dissociation of network chains in the polymer. As the temperature increases above 50 °C, **SPU1**transitions to the viscous domain [37]. The phase-angle curve of **SPU2** shows a broad relaxation in the regime from 50 °C to 100 °C corresponding to the disorder of the polymer chains. In addition, the G′ exhibits a significant rise in the rubbery plateau properties with increasing temperature above 180 °C as a result of the single amide unit in the end caps of the polymer. Interestingly, **SPU3**, which has two amide groups in the structure of the end-cap (**3b**), shows an approximately constant rubbery plateau of G′ between 0 °C and 100 °C. A crossover between G′ and loss modulus (G″) was observed at 161 °C owing to the transition of the polymer from a viscoelastic solid to a viscous liquid, and this relaxation can be attributed to the strong association that leads to the hard region in the structure of the polymer. Rheological analysis of **SPU4** revealed two relaxations: the first in the range between 60 °C and 70 °C, corresponding to the internal relaxation, and the second between 77 °C and 81 °C, resulting from the change in polymer behaviour from a viscoelastic solid to a viscous liquid. The crossover between G′ and G″ for **SPU5** shifted to 103.5 °C and **SPU6** showed a broad simple relaxation between 120 °C and 160 °C as a result of an internal transition, which indicates the high degree of association between the chains of the supramolecular polymers, in turn attributed to the amide motifs in their structure.

The extended rubbery characteristics of **SPU2**, **SPU3**, **SPU5** and **SPU6** were observed at high temperature as a result of the strong association of amide units in the supramolecular polymers. Thus, the polymers remain stiffer, while **SPU1** and **SPU4** exhibit viscoelastic properties because of the absence of amide end capping motifs in their structure.

To understand further the mechanical properties of the prepared SPUs, tensile testing was performed, as shown in Fig. 4 and Table 2. The comparisons between **SPU1**, **SPU2**, and **SPU3**, which contain the morpholine moiety in the end-caps, show significant enhancement in the Young's modulus (YM), ultimate tensile strength (UTS), and modulus of toughness (MoT), but a drastic decrease in the elongation at break (EB) after the introduction of amide units in the end caps of the supramolecular polymers. These changes in the mechanical properties of the polymers are attributed to the strong association between the polymer chains via hydrogen bonding and this association leads to significant improvement in the stiffness of each material. However, this same trend is not seen with **SPU4**, **SPU5** and-**SPU6**, which contain an alkyl chain in the end-cap. **SPU6**, which has an end-cap comprising of two amide motifs and an alkyl end group, shows a considerable increase in the resistance of polymer deformation under loading (YM) of 19.2 ± 0.3 MPa when compared to **SPU5** with one amide, which has a YM value of 7.8 ± 0.2 MPa, and **SPU4** which is without an amide functional group and has a YM of 7.1 ± 1.1 MPa. **SPU6** shows a slight increase in EB when compared to **SPU5** and **SPU4**. In contrast, the UTS and MoT of **SPU6** of 4.2 ± 0.07 MPa and 3.1 ± 0.05 MJm^{-3}, respectively, were the highest values observed in this study. Strikingly, the mechanical characterisation of **SPU6** was enhanced in both tensile strength and elongation. This behaviour could reflect the dynamic nature of the polymer chains, which is reinforced by strong hydrogen-bonding interactions between the

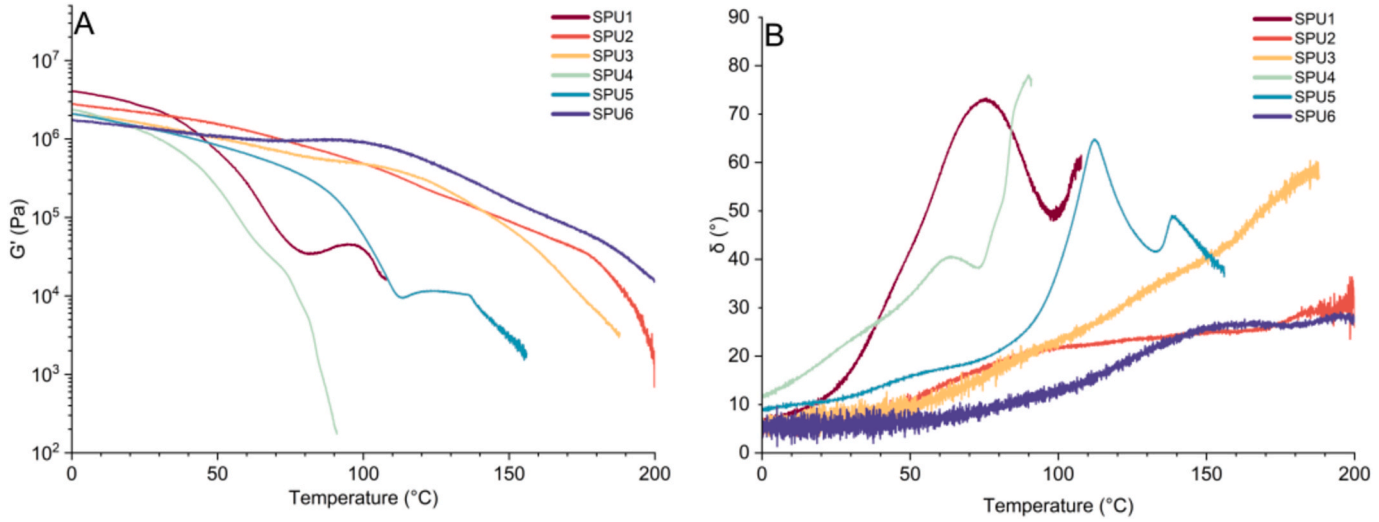

Fig. 3. The rheological behaviour of **SPU1**-**SPU6** over the temperature range of 0–200 °C, at a heating rate of 2 °C min^{-1}, using a normal force of 1 N and a frequency of 1 Hz. (A) storage modulus (G′) against temperature, (B) phase angle (δ) against temperature.

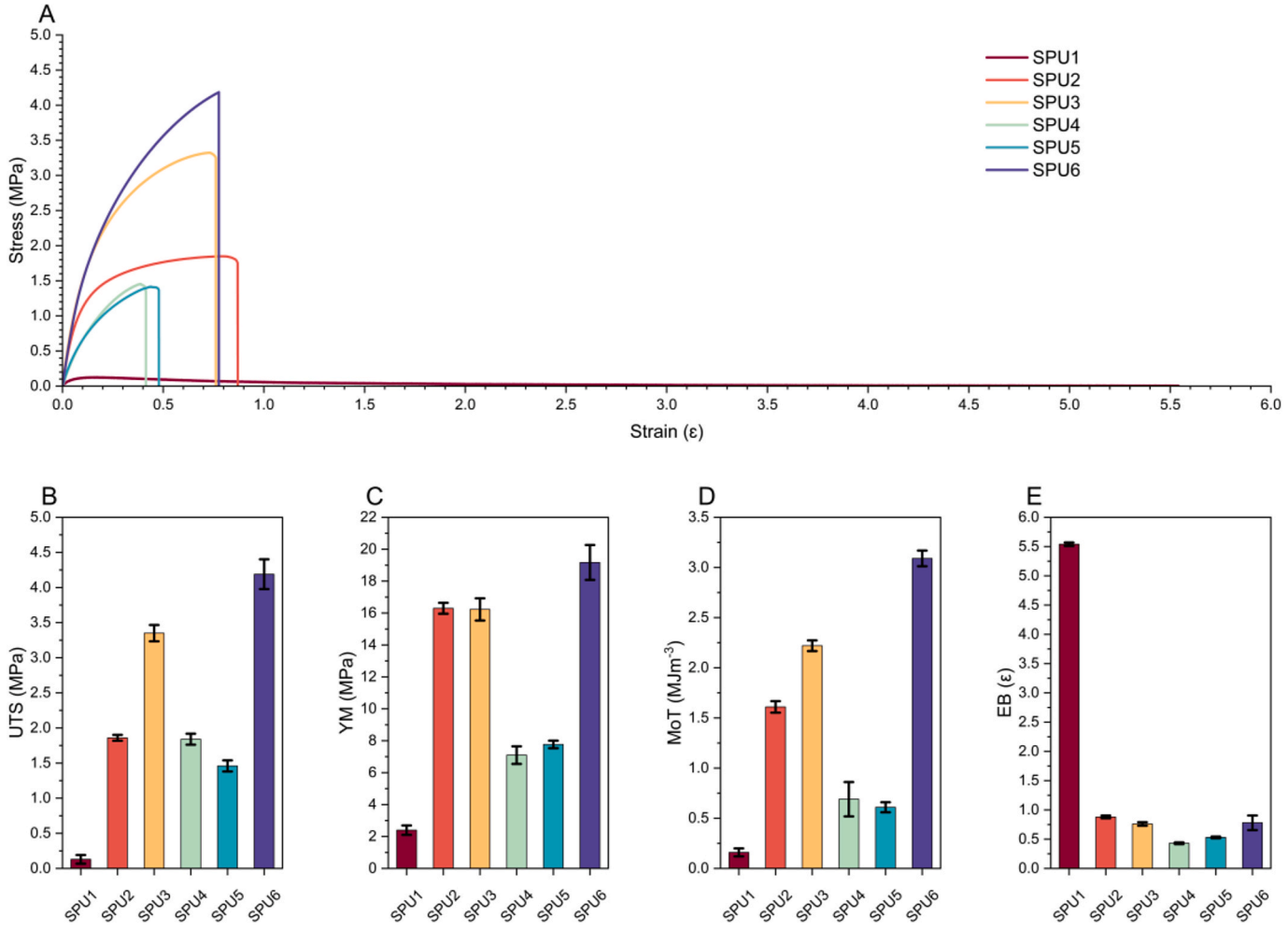

Fig. 4. Mechanical properties of **SPU1**-**SPU6**, (A) Tensile stress-strain curves of the SPUs, (B) Ultimate Tensile Strength (UTS), (C) Young's modulus (YM), (D) Modulus of toughness (MoT), and (E) elongation at break (EB). The error shown is the standard deviation (values shown are the averages of 3 repeat measurements for each sample).

Table 2
Effect of polymer end-caps on the mechanical properties of the SPUs; the values recorded are the averages of three separate samples for each SPU. The error shown is the standard deviation for the three repeat measurements for each sample.

SPU	UTS (MPa)	EB (ε)	YM (MPa)	MoT (MJm^{-3})
SPU1	0.1 ± 0.02	5.5 ± 0.3	2.4 ± 0.04	0.2 ± 0.01
SPU2	1.9 ± 0.04	1.0 ± 0.02	16.3 ± 0.6	1.6 ± 0.05
SPU3	3.6 ± 0.1	0.9 ± 0.03	16.3 ± 0.7	2.2 ± 0.2
SPU4	1.8 ± 0.2	0.6 ± 0.02	7.1 ± 1.1	0.7 ± 0.07
SPU5	1.5 ± 0.03	0.6 ± 0.02	7.8 ± 0.2	0.6 ± 0.07
SPU6	5.2 ± 0.07	0.9 ± 0.01	19.2 ± 0.3	3.1 ± 0.05

carbonyl moieties and the N–H units in the amide–urea and amide–amide associations as shown in the solid-state structure of the **SPU6** end-cap (**4f**) (see Fig. S64 and Table S17).

Variable-temperature infrared (VT-IR) spectroscopic analysis was conducted on **SPU4**, **SPU5**, and **SPU6** from 20 °C to 200 °C. The absorbances of the amide, urea, and urethane carbonyl groups were monitored to investigate the thermal stability and the transformation of the hydrogen-bonding interactions from associated to disassociated states as the temperature was increased [61,62], (see Fig. 5). **SPU4**, **SPU5**, and **SPU6** show strong absorbance at *ca.* 1734 cm^{-1} and *ca.* 1710 cm^{-1} corresponding to free urethane (non-hydrogen bonded) and ordered hydrogen bonded urethane groups, respectively [58,63,64]. The IR spectra of **SPU4** features bands at 1663 cm^{-1} and 1686 cm^{-1} corresponding to hydrogen bonded and free urea carbonyl group [63,65]. However, **SPU5** and **SPU6** show strong absorbance in their spectra at *ca.* 1642 cm^{-1} and *ca.* 1668 cm^{-1} related to ordered associated and non-hydrogen bonded amide and urea groups, respectively [66]. During the heating cycles, the frequency of the ordered hydrogen-bonded C═O of urethane shifted systematically to high wavenumbers at *ca.* 1746 cm^{-1} owing to the hydrogen bonds dissociating to afford free urethane [63,66,67]. This onset occurs at *ca.* 60 °C–80 °C (**SPU4**), 80 °C–120 °C (**SPU5**), and 150 °C–200 °C (**SPU6**). For **SPU4**, on increasing the temperature, the intensity of the urea absorbance band at 1663 cm^{-1} was observed to decrease, whilst the intensity of the non-hydrogen-bonded urea was seen to increase to 1692 cm^{-1}. With increasing temperature, a significant shift in the ordered hydrogen-bonded amide and urea carbonyl groups of **SPU5** and **SPU6** to the disordered hydrogen bonded state was observed, from *ca.* 1642 cm^{-1} to 1668 cm^{-1}. Subsequently the carbonyl band shifts further to *ca.* 1692 cm^{-1} corresponding to the dissociation of the hydrogen bonding interactions [68,69]. All three polymers showed shifting of the N–H bending vibration from *ca.* 1537 cm^{-1} to 1521 cm^{-1} with increasing temperature, indicating phase separation via a disassociated hydrogen bonding network [62,69]. The IR spectra of **SPU5** and **SPU6** feature a significant absorbance at 1698 cm^{-1} that can be assigned to the hydrogen-bonding interactions between

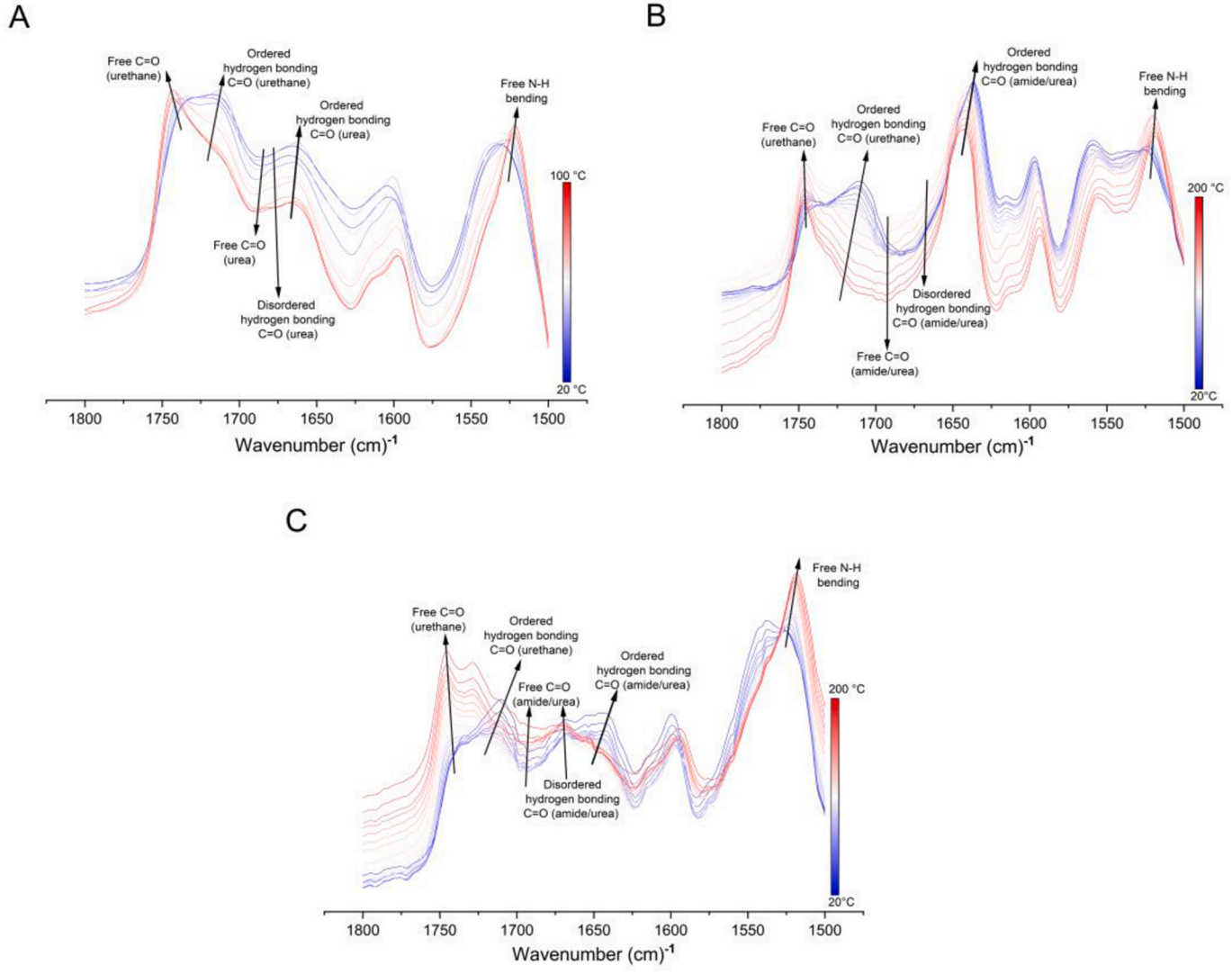

Fig. 5. VT-IR spectra in the 1500 cm^{-1} to 1800 cm^{-1} region of (A) **SPU4**, (B) **SPU5**, and (C) **SPU6**. Heating from 20 °C to 200 °C at 10 °C intervals.

C═O moieties of urethane–amide associations and urea N–H units, because the frequency of this band is slightly lower than the inter-urethane band at *ca.* 1710 cm^{-1}, which indicates that the network between the carbonyl moiety and N–H unit of the urethane is weaker than interaction between the C═O moieties of urethane–amide associations and urea N–H units [63,65,70,71].

The morphology of **SPU1**-**SPU6** was investigated using atomic force microscopy (AFM) in tapping mode. Phase and height modes are sensitive to the modules of the soft and hard domains, therefore these were used to assess the phase separation between the segments of polymer [72,73]. AFM analysis of each of the supramolecular polyurethanes revealed two phases: the first revealed to the hard segments which was observed as a deep colour (dark regions) as a result of the low phase angle, and the second phase was attributed to the soft segments (light coloured regions) corresponding to the high phase angle, as shown in Fig. 6 and Figs. S89 and S90 [74–76]. AFM phase and height images display aggregation of hard domains of the supramolecular polyurethanes [77,78]. This aggregation in the SPUs could be attributed to a phase-separation phenomenon; this phenomenon increased when amide motifs were introduced in both of the end-cap types (morpholine **SPU1**-**SPU3** and butyl **SPU4**-**SPU6**) of the polymer resulting in a high degree of association between polymer chains [79]. The average size of the aggregates of the hard segment decreases from **SPU1** to **SPU3** (i.e. morpholine end-caps), corresponding to the enhanced interaction of polymer chains via hydrogen bonding, while the phase separation became more evident from **SPU4** (has diameters around *ca.* 0.2–0.4 μm) to **SPU6** (has diameters around *ca.* 0.7–0.9 μm) (i.e. alkyl end-caps) [80]. Preliminary SAXS analyses revealed phase-separated morphologies for these SPUs on the nanometer scale (see Fig. S91) in agreement with analogous SPU derivatives that we have reported previously [50,56]. In addition, it was evident from these studies that the non-covalent interactions of both of the end caps (see Fig. S89) led to ordered nanostructures—these assemblies are the subject of further studies by SAXS analysis to establish the effect of the structure of the end-caps on the ordered morphologies. Furthermore, the absence of crystalline domains in these SPUs was confirmed by WAXS analysis (see Fig. S92) [81]. However, the SPU derivatives with ordered nanostructure featured a weak reflection in the WAXS profiles centered around 17.3 nm that suggest that π-π stacking (3.5 Å) interactions between the end-caps aid the organization of the molecular packing of the hard segments.

An optical microscope equipped with a hot stage was used to investigate the morphology and self-healing capability of SPUs between 20 °C and 250 °C, with the heating rate of 10 °C min^{-1}. The polymer film was cut into two parts using a scalpel blade and healed with an increase in the temperature, as shown in Fig. 7 (and Supporting Information (SI), videos S1–S6). Healing of **SPU4** was observed at approximately 75 °C and the gap between two pieces progressively disappeared with increasing temperature with full closure of the damage achieved at 90 °C, indicating that mobility of the molecular chains increased gradually with temperature. In the case of **SPU5**, healing began at about 105 °C and the damaged area completely vanished at 140 °C — traces of the cut were almost invisible. In contrast, **SPU6** was monitored, and healing became evident only at elevated temperatures (*ca.* 200 °C) where there was sufficient energy to increase the intensity of molecular chain motions. Complete healing was attained at 218 °C. Indeed, the healing progress of **SPU5** and **SPU6** required higher temperatures as result of the presence of amide motifs in the end-caps of the polymer. The elevated temperatures required to induce healing are attributed to the increased levels of hydrogen bonding and the phase separation between the polymer chains, which is consistent with the AFM and rheological analysis of these materials.

In contrast to the previously reported behaviour of structurally related SPUs [25,37], **SPU2**, **SPU3**, **SPU5**, and **SPU6** did not self-heal at temperatures below 100 °C as a consequence of the abundance of the strong hydrogen-bond forming amide units in their end-cap structures. The abundance of hydrogen bonds hinders the mobility of soft and hard molecular segments by decreasing the free volume between the polymer chains, which is required for self-healing ability [82,83]. These data are in agreement with the VT-IR spectroscopic results for **SPU5** and **SPU6,** which, at high temperatures, show absorbance bands in the regions

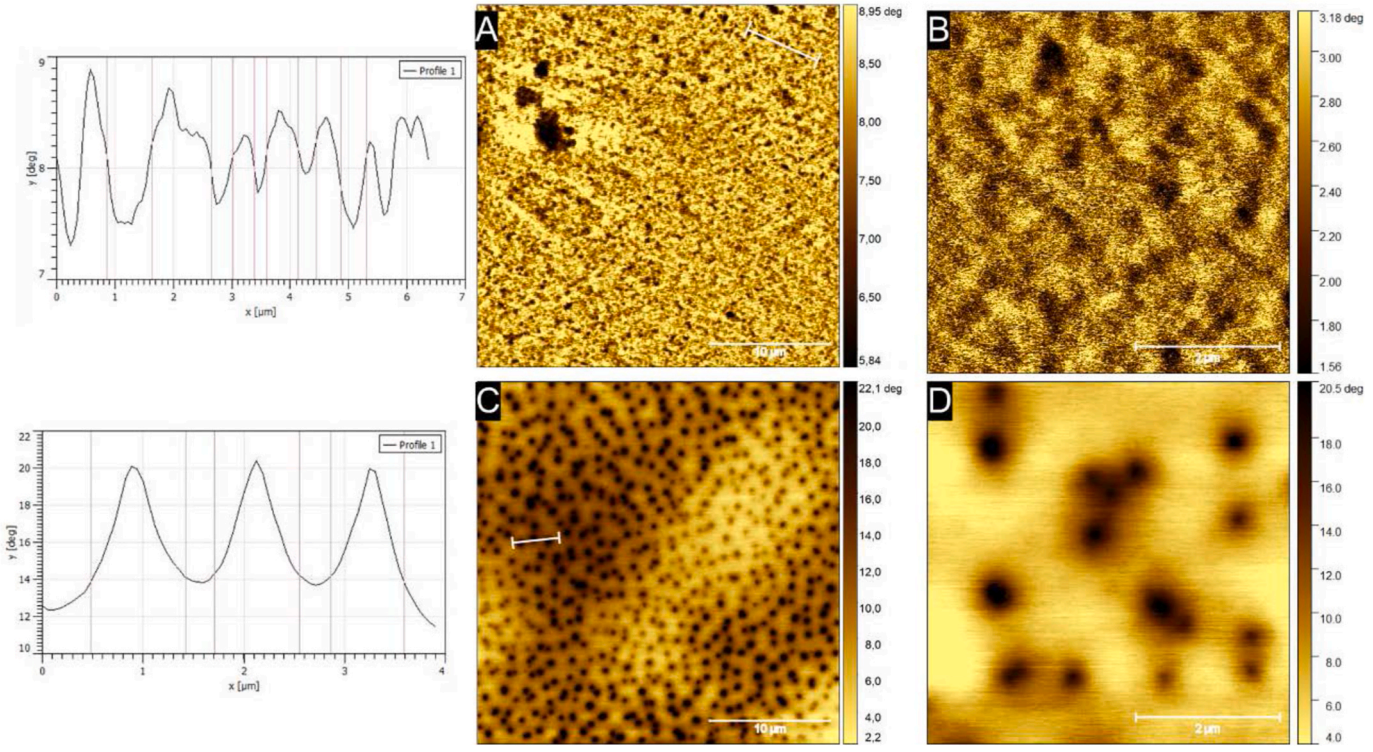

Fig. 6. AFM tapping mode phase images of resultant **SPU4** (A, B) and **SPU6** (C, D) for two different scale bars 10 μm and 2 μm. All the polymer samples were prepared by drop casting from $CHCl_3$ (0.5 mg mL^{-1}) onto a mica disc.

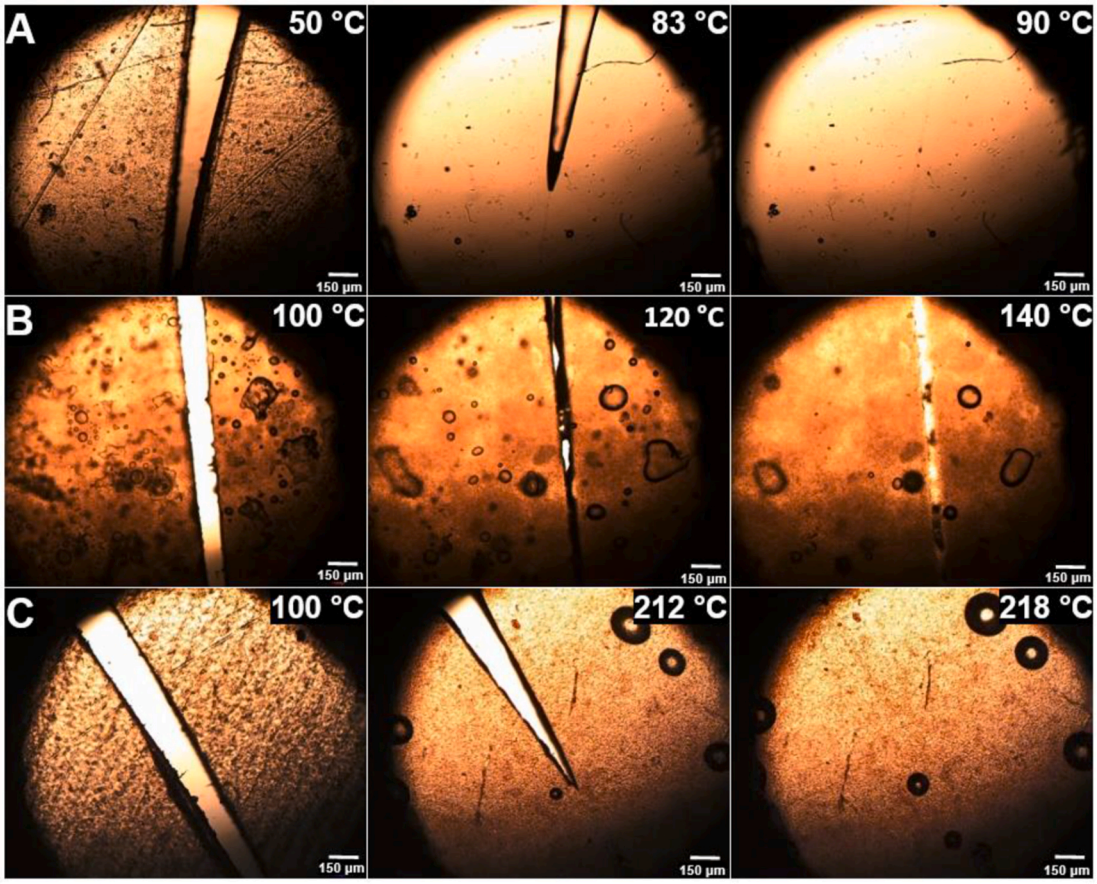

Fig. 7. Healing progress of (A) **SPU4,** (B) **SPU5**, and (c) **SPU6**. Images were taken using an optical microscope equipped with a hot stage between 20 °C and 250 °C, with the heating rate of 10 °C min^{-1}. The scale bar represents 150 μm.

1720 cm^{-1} to 1735 cm^{-1} and 1650 cm^{-1} to 1680 cm^{-1} that were attributed to the strength of the hydrogen bonding between polymer chains via urethane and urea/amide associations, respectively [84].

To demonstrate the healing efficiency of supramolecular polyurethanes upon exposure to thermal stimuli, tensile tests were conducted on pristine, annealed, and healed polymer samples (*ca.* 0.4 mm thick, 25 mm long and 5 mm wide). The healing efficiency and the stress-strain curves are summarized in Table 3 and Fig. 8 plus Table S18 and Fig. S94. To test the healing capability, the SPU samples were first cut in half with a scalpel, and then the two parts gently reattached on a pre-heated PTFE plate [85]. These damaged samples were then placed into a pre-heated oven for two different healing times (1 and 4 h) at various temperatures (the temperature used is derived from the cross-over between G′ and G″ from the rheological analysis for each polymer sample) and then cooled to room temperature for 1 h [38].

All the annealed SPUs show changes in the mechanical properties when compared to the pristine version in terms of YM and MoT as a function of time [86]. **SPU1** recovered all the mechanical properties completely (UTS and EB) after annealing and healing for 4 h, at 40 °C [37]. Good healing was observed for **SPU2**: 91 % in UTS, with an EB of 157 % after 4 h. **SPU3** exhibited a low healing efficiency of 33 % in UTS, while EB increased to 129 % for 4 h at 190 °C. Modest self-healing efficiency was achieved for **SPU5**: 49 % for UTS, with an EB of 169 % after 4 h at 160 °C. It is interesting to note that the increase in healing time of **SPU3** and **SPU5** from 1 h to 4 h did not affect the healing efficiency of the UTS of the repaired polymer but did result in an increase the EB value. The behaviour of the UTS can be attributed to the re-association of the dissociated hydrogen bonding functionalities occurring within the separate healing domains and not across the damaged interface [87]. Furthermore, it may also be as a result of over-incorporated end-caps between polymer chains at the damaged interface and weaker dynamic interactions; the above might disturb the hydrogen bonds interaction which adversely effect on self-healing properties. However, the EB increase is assumed to be attributed to melting the hard regions and the segments started to move and increase the chains mobility [88,89]. Poor self-healing efficiency of **SPU4** in comparison to **SPU1** corresponds to low re-association between the polymer chains which possesses an alkyl end group [56]. In contrast, by increasing the number of amide groups in the end-caps of the SPUs, healing was not observed for **SPU6** as a result of the extension of the rubber plateau to more than 200 °C (Fig. 3).

Table 3
Healing efficiency of the mechanical properties of **SPU1**-**SPU6** after 4 h calculated from pristine and healed values.

SPU	Temperature (°C)	UTS (MPa)	YM (MPa)	MoT (MJm^{-3})	EB (ε)
SPU1	40	100 %	86 %	94 %	80 %
SPU2	190	91 %	32 %	71 %	157 %
SPU3	160	31 %	21 %	18 %	129 %
SPU4	50	6 %	6 %	10 %	127 %
SPU5	100	43 %	74 %	157 %	350 %
SPU6	190	–	–	–	–

The adhesive properties of the SPUs were investigated by lap shear tests using glass and aluminum substrates, see Fig. 9, Table 4, and Table S19. The polymers were placed between two slides of glass or aluminum and held by clamps from each side. The assessment of the supramolecular polymers' adhesion was conducted at two different bonding temperatures; 50 °C (**SPU1** and **SPU4**) and 160 °C (**SPU2**, **SPU3**, **SPU5**, and **SPU6**) for 30 min and then allowed to cool to room temperature for 1 h. The SPUs were then investigated for their use as reusable adhesives. Re-adhesion of **SPU1**-**SPU6** was conducted on both

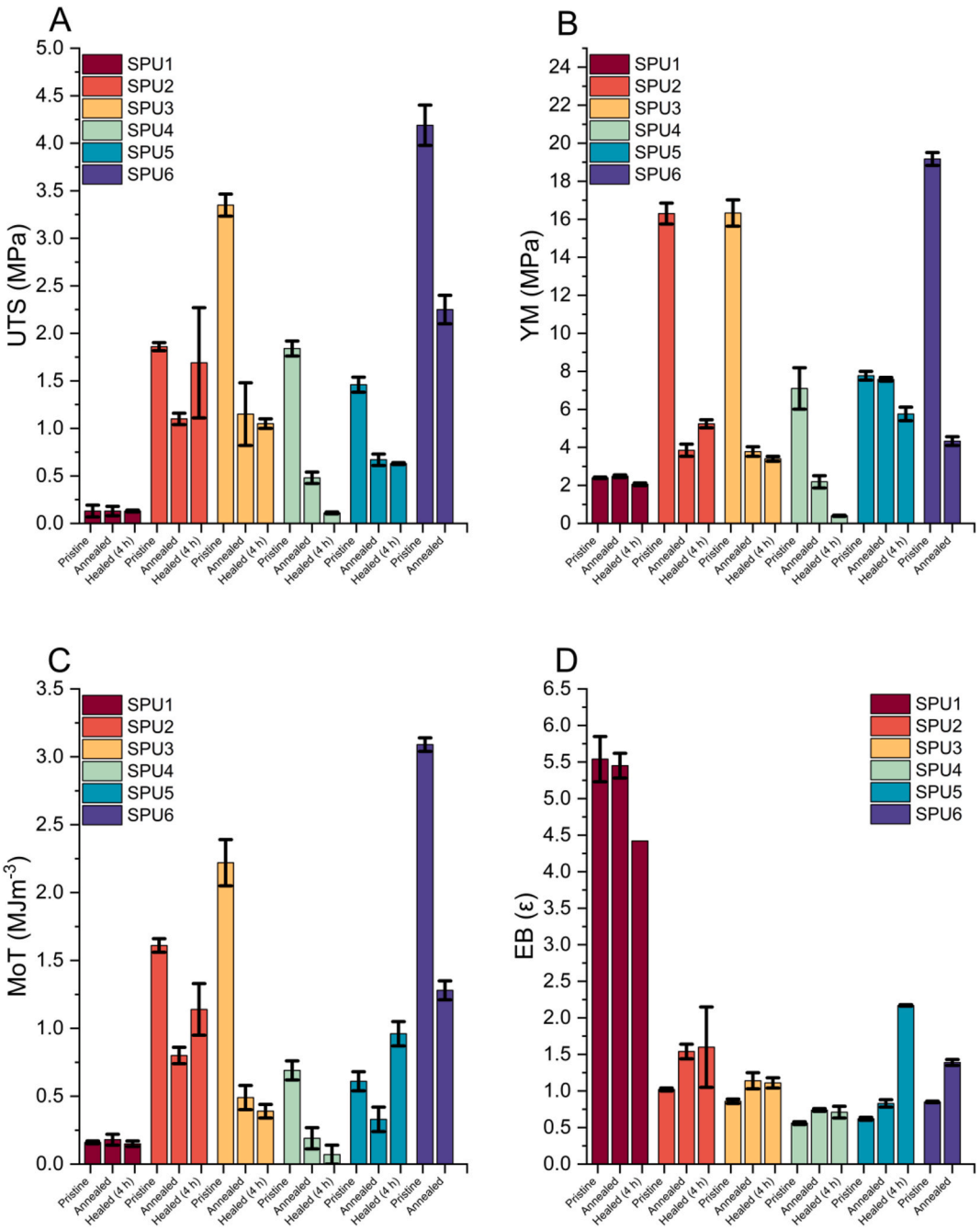

Fig. 8. Comparative mechanical properties of the pristine (left), annealed (center), and healed (4 h) (right) **SPU1**-**SPU6**, (A) Ultimate Tensile Strength (UTS), (B) Young's modulus (YM), (C) Modulus of toughness (MoT), and (D) elongation at break (EB). The error shown is the standard deviation (values shown are the average of 3 repeats for each sample).

glass and aluminium over three cycles. After three re-adhesion cycles, **SPU1**, **SPU2**, **SPU4**, and **SPU6** exhibited good re-adhesion capabilities, retaining more than 70 % of the initial shear strength when adhering to both glass and aluminum. **SPU5** showed remarkable adhesion properties exhibiting the highest shear strength on both glass (4.1 ± 0.4 MPa) and aluminum (3.8 ± 0.4 MPa) substrates. In addition, the retention of shear strength over 3 cycles was more than 90 % and 68 % in adhering to glass and aluminum, respectively. To put this in context, Lun et al. have developed healable supramolecular polyamide-urea with a maximum lap shear strength of 0.16 ± 0.01 MPa and re-adhesive capability over four cycles was 63 % of the initial strength when adhering to aluminum [90]. When adhering to glass and aluminum, **SPU4** demonstrates the lowest shear strength (0.8 ± 0.2 MPa and 0.7 ± 0.6 MPa, respectively) and re-adhesive capabilities (56 % and 43 %, respectively) as a consequence of the absence of amide end-capping motifs in the structure and the inactive hydrogen-bonding alkyl group.

4. Conclusions

In this study, we have successfully designed and synthesised several novel aliphatic amide end-cap units, which were then used to construct new self-healing supramolecular polyurethanes. The effect of these end-caps on the thermal and mechanical properties plus rheological behaviour of supramolecular polyurethanes was then investigated. A systematic correlation between a variety of physical and mechanical characteristics, for example Tm, phase separation, viscoelastic

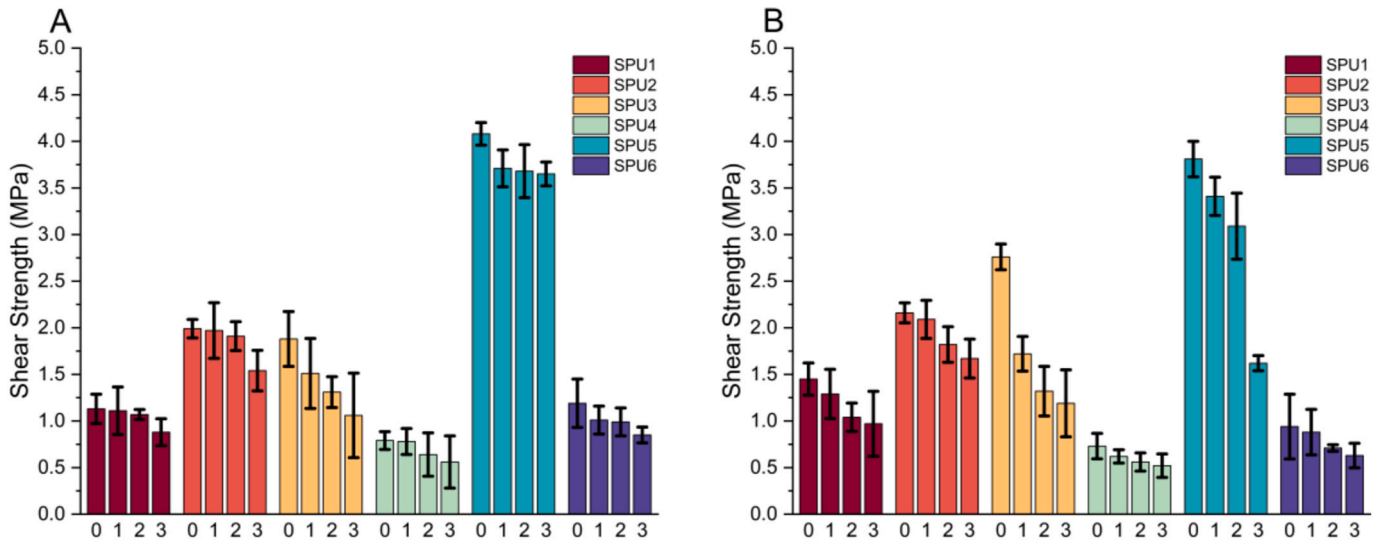

Fig. 9. Comparison of the shear strength of **SPU1-SPU6** over three re-adhesion cycles. Lap shear strength on (A) glass and (B) aluminum.

Table 4
Shear strength efficiency of SPUs on glass and aluminum after three re-adhesion cycles. The error shown is the standard error (values shown are calculated from the averages of the 3 repeats of the pristine material (cycle 0) and re-adhesion (cycle 3)).

SPU	Glass	Aluminium
SPU1	77 ± 16 %	67 ± 25 %
SPU2	77 ± 7 %	78 ± 7 %
SPU3	57 ± 34 %	43 ± 14 %
SPU4	71 ± 22 %	70 ± 24 %
SPU5	90 ± 3 %	43 ± 5 %
SPU6	71 ± 23 %	67 ± 31 %

transition, shear strength, and the type and strength of hydrogen bonding in the end-caps was found. The rheological behaviour of the SPUs was enhanced by the association between polymer chains within the amide end-caps which resulted in extension of the rubbery plateau. The mechanical properties of **SPU2**, **SPU3**, **SPU5**, and **SPU6** were enhanced after introduction of the amide groups. **SPU3** shows an increase of YM and UTS by 274 %, and 1046 %, respectively, when compared to **SPU1**. **SPU6** exhibited increased UTS and YM, by 277 % and 270 %, respectively, when compared to **SPU4**. AFM verified the phase separation in the SPUs and revealed that the incompatibility between the soft domain and hard domain increased with amide groups in the end-caps of the polymer, leading to reinforced rheological, mechanical, and thermal properties. Furthermore, upon exposure to thermal stimuli these SPUs illustrated the ability to undergo healing as well as provide good re-adhesive properties on both glass and aluminum substrates, with **SPU2** exhibiting a retention of shear strength of 77 % and 78 % after three re-adhesion cycles on glass and aluminum, respectively.

CRediT authorship contribution statement

Alarqam Z. Tareq: Writing – original draft, Validation, Investigation, Formal analysis, Conceptualization. **Matthew Hyder:** Conceptualization, Formal analysis, Investigation, Visualization. **Daniel Hermida Merino:** Formal analysis, Writing – review & editing. **Ann M. Chippindale:** Formal analysis, Writing – review & editing. **Amanpreet Kaur:** Writing – review & editing, Formal analysis. **James A. Cooper:** Writing – review & editing, Supervision. **Wayne Hayes:** Writing – review & editing, Supervision, Resources, Project administration, Conceptualization.

Declaration of competing interest

The authors declare that they have no known competing financial interests or personal relationships that could have appeared to influence the work reported in this paper.

Data availability

Data will be made available on request.

Acknowledgements

The authors would like to acknowledge the financial support from HCED Iraq (PhD studentship for A.Z.T.) and from the University of Reading and Domino Printing Sciences Ltd (PhD studentship for M.H.). In addition, the University of Reading (EPSRC – Doctoral Training Grant) is acknowledged for providing access to instrumentation in the Chemical Analysis Facility. We thank Total Cray Valley for the kind supply of (hydrogenated poly(butadiene) Krasol™ HLBH-P 2000 and Mr Nick Spencer (Chemical Analysis Facility (CAF), University of Reading) for collecting the single-crystal X-ray data.

Appendix A. Supplementary data

Supplementary data to this article can be found online at https://doi.org/10.1016/j.polymer.2024.127052.

References

[1] P. Cordier, F. Tournilhac, C. Soulié-Ziakovic, L. Leibler, Self-healing and thermoreversible rubber from supramolecular assembly, Nature 451 (7181) (2008) 977–980.
[2] M. Burnworth, L. Tang, J.R. Kumpfer, A.J. Duncan, F.L. Beyer, G.L. Fiore, S. J. Rowan, C. Weder, Optically healable supramolecular polymers, Nature 472 (7343) (2011) 334–337.
[3] S. Salimi, L.R. Hart, A. Feula, D. Hermida-Merino, A.B.R. Touré, E.A. Kabova, L. Ruiz-Cantu, D.J. Irvine, R. Wildman, K. Shankland, W. Hayes, Property enhancement of healable supramolecular polyurethanes, Eur. Polym. J. 118 (2019) 88–96.
[4] S. Burattini, B.W. Greenland, D.H. Merino, W. Weng, J. Seppala, H.M. Colquhoun, W. Hayes, M.E. MacKay, I.W. Hamley, S.J. Rowan, A healable supramolecular polymer blend based on aromatic π-π Stacking and hydrogen-bonding interactions, J. Am. Chem. Soc. 132 (34) (2010) 12051–12058.
[5] B.A.G. Lamers, M.H.C. Van Son, F.V. De Graaf, B.W.L. Van Den Bersselaar, B.F. M. De Waal, K. Komatsu, H. Sato, T. Aida, J.A. Berrocal, A.R.A. Palmans, G. Vantomme, S.C.J. Meskers, E.W. Meijer, Tuning the donor-acceptor interactions in phase-segregated block molecules, Mater. Horiz. 9 (1) (2022) 294–302.

[6] A. Campanella, D. Döhler, W.H. Binder, Self-healing in supramolecular polymers, Macromol. Rapid Commun. (2018) 1700739.
[7] Z. Deng, Y. Guo, X. Zhao, P.X. Ma, B. Guo, Multifunctional stimuli-responsive hydrogels with self-healing, high conductivity, and rapid recovery through host-guest interactions, Chem. Mater. 30 (5) (2018) 1729–1742.
[8] H. Yang, B. Yuan, X. Zhang, O.A. Scherman, Supramolecular chemistry at interfaces: host-guest interactions for fabricating multifunctional biointerfaces, Accounts Chem. Res. 47 (7) (2014) 2106–2115.
[9] E.B. Murphy, F. Wudl, The world of smart healable materials, Prog. Mater. Sci. (2010) 223–251.
[10] Y.L. Rao, A. Chortos, R. Pfattner, F. Lissel, Y.C. Chiu, V. Feig, J. Xu, T. Kurosawa, X. Gu, C. Wang, M. He, J.W. Chung, Z. Bao, Stretchable self-healing polymeric dielectrics cross-linked through metal-ligand coordination, J. Am. Chem. Soc. 138 (18) (2016) 6020–6027.
[11] M.T. Nguyen, C.A. Pignedoli, M. Treier, R. Fasel, D. Passerone, The role of van der Waals interactions in surface-supported supramolecular networks, Phys. Chem. Chem. Phys. 12 (4) (2010) 992–999.
[12] A. Lari, R. Gleiter, F. Rominger, Supramolecular organization based on van der Waals forces: Syntheses and solid state structures of isomeric [6.6] cyclophanes with 2,5-diselenahex-3-yne bridges, Eur. J. Org. Chem. (14) (2009) 2267–2274.
[13] L.M. De Espinosa, G.L. Fiore, C. Weder, E. Johan Foster, Y.C. Simon, Healable supramolecular polymer solids, Prog. Polym. Sci. (2015) 60–78.
[14] T. Ware, K. Hearon, A. Lonnecker, K.L. Wooley, D.J. Maitland, W. Voit, Triple-shape memory polymers based on self-complementary hydrogen bonding, Macromolecules 45 (2) (2012) 1062–1069.
[15] D. Habault, H. Zhang, Y. Zhao, Light-triggered self-healing and shape-memory polymers, Chem. Soc. Rev. 42 (17) (2013) 7244–7256.
[16] S. Burattini, H.M. Colquhoun, J.D. Fox, D. Friedmann, B.W. Greenland, P.J. F. Harris, W. Hayes, M.E. MacKay, S.J. Rowan, A self-repairing, supramolecular polymer system: healability as a consequence of donor-acceptor π-π Stacking interactions, Chem. Commun. (44) (2009) 6717–6719.
[17] G. Chang, L. Yang, J. Yang, M.P. Stoykovich, X. Deng, J. Cui, D. Wang, High-performance pH-switchable supramolecular thermosets via cation–π interactions, Adv. Mater. 30 (7) (2018) 1704234.
[18] H. Chen, Y. Liu, T. Gong, L. Wang, K. Zhao, S. Zhou, Use of intermolecular hydrogen bonding to synthesize triple-shape memory supermolecular composites, RSC Adv. 3 (19) (2013) 7048–7056.
[19] S. Salimi, T.S. Babra, G.S. Dines, S.W. Baskerville, W. Hayes, B.W. Greenland, Composite polyurethane adhesives that debond-on-demand by hysteresis heating in an oscillating magnetic field, Eur. Polym. J. 121 (2019) 109264.
[20] Y. Jiang, C. Hu, H. Cheng, C. Li, T. Xu, Y. Zhao, H. Shao, L. Qu, Spontaneous, straightforward fabrication of partially reduced graphene oxide–polypyrrole composite films for versatile actuators, ACS Nano 10 (4) (2016) 4735–4741.
[21] H. Chen, Y. Li, Y. Liu, T. Gong, L. Wang, S. Zhou, Highly pH-sensitive polyurethane exhibiting shape memory and drug release, Polym. Chem. 5 (17) (2014) 5168–5174.
[22] A.D. Odonnell, A.G. Gavriel, W. Christie, A.M. Chippindale, I.M. German, W. Hayes, Conformational control of bis-urea self-assembled supramolecular pH switchable low-molecular-weight hydrogelators, ARKIVOC (Gainesville, FL, U. S.) 2021 (6) (2021) 222–241.
[23] D. Gao, G. Thangavel, J. Lee, J. Lv, Y. Li, J.-H. Ciou, J. Xiong, T. Park, P.S. Lee, A supramolecular gel-elastomer system for soft iontronic adhesives, Nat. Commun. 14 (1) (2023) 1990.
[24] C.B. Cooper, S. Nikzad, H. Yan, Y. Ochiai, J.C. Lai, Z. Yu, G. Chen, J. Kang, Z. Bao, High energy density shape memory polymers using strain-induced supramolecular nanostructures, ACS Cent. Sci. 7 (10) (2021) 1657–1667.
[25] A. Feula, A. Pethybridge, I. Giannakopoulos, X. Tang, A. Chippindale, C.R. Siviour, C.P. Buckley, I.W. Hamley, W. Hayes, A thermoreversible supramolecular polyurethane with excellent healing ability at 45 °c, Macromolecules 48 (17) (2015) 6132–6141.
[26] S. Chen, L. Sun, X. Zhou, Y. Guo, J. Song, S. Qian, Z. Liu, Q. Guan, E. Meade Jeffries, W. Liu, Y. Wang, C. He, Z. You, Mechanically and biologically skin-like elastomers for bio-integrated electronics, Nat. Commun. 11 (1) (2020) 1107.
[27] L.R. Hart, N.A. Nguyen, J.L. Harries, M.E. Mackay, H.M. Colquhoun, W. Hayes, Perylene as an electron-rich moiety in healable, complementary π–π stacked, supramolecular polymer systems, Polymer 69 (2015) 293–300.
[28] M.J. Webber, E.A. Appel, E.W. Meijer, R. Langer, Supramolecular biomaterials, Nat. Mater. (2015) 13–26.
[29] A.D. O'Donnell, S. Salimi, L.R. Hart, T.S. Babra, B.W. Greenland, W. Hayes, Applications of supramolecular polymer networks, React. Funct. Polym. (2022) 105209.
[30] L.R. Hart, S. Li, C. Sturgess, R. Wildman, J.R. Jones, W. Hayes, 3D printing of biocompatible supramolecular polymers and their composites, ACS Appl. Mater. Interfaces 8 (5) (2016) 3115–3122.
[31] X. Kuang, K. Chen, C.K. Dunn, J. Wu, V.C.F. Li, H.J. Qi, 3D printing of highly stretchable, shape-memory, and self-healing elastomer toward novel 4D printing, ACS Appl. Mater. Interfaces 10 (8) (2018) 6841–6848.
[32] J. Yu, Y. Zhang, Y. Ye, R. DiSanto, W. Sun, D. Ranson, F.S. Ligler, J.B. Buse, Z. Gu, Microneedle-array patches loaded with hypoxia-sensitive vesicles provide fast glucose-responsive insulin delivery, Proc. Natl. Acad. Sci. USA 112 (27) (2015) 8260–8265.
[33] M. Wei, Y. Gao, X. Li, M.J. Serpe, Stimuli-responsive polymers and their applications, Polym. Chem. 8 (1) (2017) 127–143.
[34] J. Hu, R. Yang, L. Zhang, Y. Chen, X. Sheng, X. Zhang, Robust, transparent, and self-healable polyurethane elastomer via dynamic crosslinking of phenol-carbamate bonds, Polymer 222 (2021) 123674.
[35] Q. Wei, C. Schlaich, S. Prévost, A. Schulz, C. Böttcher, M. Gradzielski, Z. Qi, R. Haag, C.A. Schalley, Supramolecular polymers as surface coatings: rapid fabrication of healable superhydrophobic and slippery surfaces, Adv. Mater. 26 (43) (2014) 7358–7364.
[36] A.D. O'Donnell, S. Salimi, L.R. Hart, T.S. Babra, B.W. Greenland, W. Hayes, Applications of supramolecular polymer networks, React. Funct. Polym. 172 (2022) 105209.
[37] A. Feula, X. Tang, I. Giannakopoulos, A.M. Chippindale, I.W. Hamley, F. Greco, C. Paul Buckley, C.R. Siviour, W. Hayes, An adhesive elastomeric supramolecular polyurethane healable at body temperature, Chem. Sci. 7 (7) (2016) 4291–4300.
[38] M. Hyder, A.D. O'Donnell, A.M. Chippindale, I.M. German, J.L. Harries, O. Shebanova, I.W. Hamley, W. Hayes, Tailoring viscoelastic properties of dynamic supramolecular poly(butadiene)-based elastomers, Mater. Today Chem. 26 (2022) 101008.
[39] A.W. Bosman, R.P. Sijbesma, E.W. Meijer, Supramolecular polymers at work, Mater, Today Off. 7 (4) (2004) 34–39.
[40] R.P. Sijbesma, F.H. Beijer, L. Brunsveld, B.J.B. Folmer, J.H.K.K. Hirschberg, R.F. M. Lange, J.K.L. Lowe, E.W. Meijer, Reversible polymers formed from self-complementary monomers using quadruple hydrogen bonding, Science 278 (5343) (1997) 1601–1604.
[41] Y. Zhu, J. Hu, Y. Liu, Shape memory effect of thermoplastic segmented polyurethanes with self-complementary quadruple hydrogen bonding in soft segments, Eur. Phys. J. E 28 (1) (2009) 3–10.
[42] C.A. Harper, Handbook of Plastics, Elastomers, and Composites, McGraw-Hill Education, 2002.
[43] T.J. Touchet, E.M. Cosgriff-Hernandez, 1 - hierarchal structure–property relationships of segmented polyurethanes, in: S.L. Cooper, J. Guan (Eds.), Advances in Polyurethane Biomaterials, Woodhead Publishing, 2016, pp. 3–22.
[44] N.B. Shelke, R.K. Nagarale, S.G. Kumbar, Chapter 7 - polyurethanes, in: S. G. Kumbar, C.T. Laurencin, M. Deng (Eds.), Natural and Synthetic Biomedical Polymers, Elsevier, Oxford, 2014, pp. 123–144.
[45] D.H. Merino, A. Feula, K. Melia, A.T. Slark, I. Giannakopoulos, C.R. Siviour, C. P. Buckley, B.W. Greenland, D. Liu, Y. Gan, P.J. Harris, A.M. Chippindale, I. W. Hamley, W. Hayes, A systematic study of the effect of the hard end-group composition on the microphase separation, thermal and mechanical properties of supramolecular polyurethanes, Polymer 107 (2016) 368–378.
[46] X. Jin, N. Guo, Z. You, Y. Tan, Design and performance of polyurethane elastomers composed with different soft segments, Materials 13 (21) (2020).
[47] L.T.J. Korley, B.D. Pate, E.L. Thomas, P.T. Hammond, Effect of the degree of soft and hard segment ordering on the morphology and mechanical behavior of semicrystalline segmented polyurethanes, Polymer 47 (9) (2006) 3073–3082.
[48] S. Burattini, H.M. Colquhoun, B.W. Greenland, W. Hayes, M. Wade, Pyrene-functionalised, alternating copolyimide for sensing nitroaromatic compounds, Macromol. Rapid Commun. 30 (6) (2009) 459–463.
[49] P. Woodward, A. Clarke, B.W. Greenland, D. Hermida Merino, L. Yates, A.T. Slark, J.F. Miravet, W. Hayes, Facile bisurethane supramolecular polymers containing flexible alicyclic receptor units, Soft Matter 5 (10) (2009) 2000–2010.
[50] D.H. Merino, A.T. Slark, H.M. Colquhoun, W. Hayes, I.W. Hamley, Thermo-responsive microphase separated supramolecular polyurethanes, Polym. Chem. 1 (8) (2010) 1263–1271.
[51] P.R.O. CrysAlis, Rigaku OD, Rigaku Oxford Diffraction Ltd, Yarnton, Oxfordshire, England, 2019.
[52] L. Palatinus, G. Chapuis, Superflip - a computer program for the solution of crystal structures by charge flipping in arbitrary dimensions, J. Appl. Crystallogr. 40 (4) (2007) 786–790.
[53] P.W. Betteridge, J.R. Carruthers, R.I. Cooper, K. Prout, D.J. Watkin, CRYSTALS version 12: software for guided crystal structure analysis, J. Appl. Crystallogr. 36 (6) (2003) 1487.
[54] E. Guénin, M. Monteil, N. Bouchemal, T. Prangé, M. Lecouvey, Syntheses of phosphonic esters of alendronate, pamidronate and neridronate, Eur. J. Org. Chem. 20 (2007) 3380–3391.
[55] M.G.J. Baud, T. Leiser, P. Haus, S. Samlal, A.C. Wong, R.J. Wood, V. Petrucci, M. Gunaratnam, S.M. Hughes, L. Buluwela, F. Turlais, S. Neidle, F.J. Meyer-Almes, A.J.P. White, M.J. Fuchter, Defining the mechanism of action and enzymatic selectivity of psammaplin A against its epigenetic targets, J. Med. Chem. 55 (4) (2012) 1731–1750.
[56] P.J. Woodward, D.H. Merino, B.W. Greenland, I.W. Hamley, Z. Light, A.T. Slark, W. Hayes, Hydrogen bonded supramolecular elastomers: correlating hydrogen bonding strength with morphology and rheology, Macromolecules 43 (5) (2010) 2512–2517.
[57] D. Hermida-Merino, L.R. Hart, P.J. Harris, A.T. Slark, I.W. Hamley, W. Hayes, The effect of chiral end groups on the assembly of supramolecular polyurethanes, Polym. Chem. 12 (31) (2021) 4488–4500.
[58] D. Hermida-Merino, B. O'Driscoll, L.R. Hart, P.J. Harris, H.M. Colquhoun, A. T. Slark, C. Prisacariu, I.W. Hamley, W. Hayes, Enhancement of microphase ordering and mechanical properties of supramolecular hydrogen-bonded polyurethane networks, Polym. Chem. 9 (24) (2018) 3406–3414.
[59] X. Tang, A. Feula, B.C. Baker, K. Melia, D. Hermida Merino, I.W. Hamley, C. P. Buckley, W. Hayes, C.R. Siviour, A dynamic supramolecular polyurethane network whose mechanical properties are kinetically controlled, Polymer 133 (2017) 143–150.
[60] H. Chen, L.R. Hart, W. Hayes, C.R. Siviour, Mechanical characterisation and modelling of a thermoreversible superamolecular polyurethane over a wide range of rates, Polymer 221 (2021) 123607.

[61] K. Zhang, A.M. Nelson, S.J. Talley, M. Chen, E. Margaretta, A.G. Hudson, R. B. Moore, T.E. Long, Non-isocyanate poly(amide-hydroxyurethane)s from sustainable resources, Green Chem. 18 (17) (2016) 4667–4681.
[62] K. Zhang, M. Aiba, G.B. Fahs, A.G. Hudson, W.D. Chiang, R.B. Moore, M. Ueda, T. E. Long, Nucleobase-functionalized acrylic ABA triblock copolymers and supramolecular blends, Polym. Chem. 6 (13) (2015) 2434–2444.
[63] L. Ning, W. De-Ning, Y. Sheng-Kang, Hydrogen bonding between urethane and urea: band assignment for the carbonyl region of FTi.r. spectrum, Polymer 37 (14) (1996) 3045–3047.
[64] M.M. Coleman, K.H. Lee, D.J. Skrovanek, P.C. Painter, Hydrogen bonding in polymers. 4. Infrared temperature studies of a simple polyurethane, Macromolecules 19 (8) (1986) 2149–2157.
[65] L.H. Chan-Chan, G. González-García, R.F. Vargas-Coronado, J.M. Cervantes-Uc, F. Hernández-Sánchez, A. Marcos-Fernandez, J.V. Cauich-Rodríguez, Characterization of model compounds and poly(amide-urea) urethanes based on amino acids by FTIR, NMR and other analytical techniques, Eur. Polym. J. 92 (2017) 27–39.
[66] Y. Ji, X. Yang, Z. Ji, L. Zhu, N. Ma, D. Chen, X. Jia, J. Tang, Y. Cao, DFT-calculated IR spectrum amide I, II, and III band contributions of N-methylacetamide fine components, ACS Omega 5 (15) (2020) 8572–8578.
[67] M.M. Coleman, D.J. Skrovanek, J. Hu, P.C. Painter, Hydrogen bonding in polymer blends. 1. FTIR studies of urethane-ether blends, Macromolecules 21 (1) (1988) 59–65.
[68] H.S. Lee, Y.K. Wang, S.L. Hsu, Spectroscopic analysis of phase separation behavior of model polyurethanes, Macromolecules 20 (9) (1987) 2089–2095.
[69] C. Zhang, Z. Ren, Z. Yin, H. Qian, D. Ma, Amide II and amide III bands in polyurethane model soft and hard segments, Polym. Bull. 60 (1) (2008) 97–101.
[70] A. Genovese, R.A. Shanks, Simulation of the specific interactions between polyamide-6 and a thermoplastic polyurethane, Comput. Theor. Polym. Sci. 11 (1) (2001) 57–62.
[71] C. Wu, J. Wang, P. Chang, H. Cheng, Y. Yu, Z. Wu, D. Dong, F. Zhao, Polyureas from diamines and carbon dioxide: synthesis, structures and properties, Phys. Chem. Chem. Phys. 14 (2) (2012) 464–468.
[72] Y. Yuan, S. Zhu, J. Zhu, P. Niu, A. Sun, X. Liu, L. Wei, Y. Li, An impact-strengthening, reusable hot-melt structural adhesive derived from branching polyurethane-based supramolecular topology capped by self-complementary hydrogen bonding UPy motifs, Eur. Polym. J. 196 (2023) 112253.
[73] N.E. Botterhuis, D.J.M. van Beek, G.M.L. van Gemert, A.W. Bosman, R.P. Sijbesma, Self-assembly and morphology of polydimethylsiloxane supramolecular thermoplastic elastomers, J. Polym. Sci. Polym. Chem. 46 (12) (2008) 3877–3885.
[74] D. Xiang, L. Liu, Y. Liang, Effect of hard segment content on structure, dielectric and mechanical properties of hydroxyl-terminated butadiene-acrylonitrile copolymer-based polyurethane elastomers, Polymer 132 (2017) 180–187.
[75] D. Pedrazzoli, I. Manas-Zloczower, Understanding phase separation and morphology in thermoplastic polyurethanes nanocomposites, Polymer 90 (2016) 256–263.
[76] K.L.A. Cimatu, U.I. Premadasa, T.D. Ambagaspitiya, N.M. Adhikari, J.H. Jang, Evident phase separation and surface segregation of hydrophobic moieties at the copolymer surface using atomic force microscopy and SFG spectroscopy, J. Colloid Interface Sci. 580 (2020) 645–659.
[77] H. Yan-ting, C. Zheng, D. Wei, Z. Fan, X. Zhong-yin, Comparative study of in situ polymerized waterborne polyurethane/nano-silica composites and polyethersiloxanediol-modified polyurethane, J. Thermoplast. Compos. Mater. 30 (1) (2015) 107–120.
[78] J. He, F. Song, X. Li, L. Chen, X. Gong, W. Tu, A novel kind of room temperature self-healing poly(urethane-urea) with robust mechanical strength based on aromatic disulfide, J. Polym. Res. 28 (4) (2021) 122.
[79] X. Lu, M. Xu, Y.-m. Sheng, Z.-p. Li, H.-m. Li, Preparation of polyurethanes with broad damping temperature range and self-healing properties, J. Elastomers Plast. 52 (5) (2019) 410–431.
[80] P. Du, X. Liu, Z. Zheng, X. Wang, T. Joncheray, Y. Zhang, Synthesis and characterization of linear self-healing polyurethane based on thermally reversible Diels–Alder reaction, RSC Adv. 3 (35) (2013) 15475–15482.
[81] Y. He, X. Zhang, J. Runt, The role of diisocyanate structure on microphase separation of solution polymerized polyureas, Polymer 55 (3) (2014) 906–913.
[82] N. Roy, B. Bruchmann, J.-M. Lehn, DYNAMERS: dynamic polymers as self-healing materials, Chem. Soc. Rev. 44 (11) (2015) 3786–3807.
[83] Y. Yang, M.W. Urban, Self-healing polymeric materials, Chem. Soc. Rev. 42 (17) (2013) 7446–7467.
[84] N. Roy, Z. Tomovic, E. Buhler, J.M. Lehn, An easily accessible self-healing transparent film based on a 2D supramolecular network of hydrogen-bonding interactions between polymeric chains, Chemistry 22 (38) (2016) 13513–13520.
[85] H. Wu, X. Liu, D. Sheng, Y. Zhou, S. Xu, H. Xie, X. Tian, Y. Sun, B. Shi, Y. Yang, High performance and near body temperature induced self-healing thermoplastic polyurethane based on dynamic disulfide and hydrogen bonds, Polymer 214 (2021) 123261.
[86] G.L. Wilkes, R. Wildnauer, Kinetic behavior of the thermal and mechanical properties of segmented urethanes, J. Appl. Phys. 46 (10) (2008) 4148–4152.
[87] C.-C. Cheng, F.-C. Chang, J.-K. Chen, T.-Y. Wang, D.-J. Lee, High-efficiency self-healing materials based on supramolecular polymer networks, RSC Adv. 5 (122) (2015) 101148–101154.
[88] W. Fan, Y. Jin, L. Shi, W. Du, R. Zhou, Transparent, eco-friendly, super-tough "living" supramolecular polymers with fast room-temperature self-healability and reprocessability under visible light, Polymer 190 (2020) 122199.
[89] J. Xu, P. Chen, J. Wu, P. Hu, Y. Fu, W. Jiang, J. Fu, Notch-Insensitive, ultrastretchable, efficient self-healing supramolecular polymers constructed from multiphase active hydrogen bonds for electronic applications, Chem. Mater. 31 (19) (2019) 7951–7961.
[90] L. Zhang, D. Wang, L. Xu, A. Zhang, A supramolecular polymer with ultra-stretchable, notch-insensitive, rapid self-healing and adhesive properties, Polym. Chem. 12 (5) (2021) 660–669.